doi:10.1093/brain/awz169 BRAIN 2019: 142; 2288–2302 | 2288

BRAIN
A JOURNAL OF NEUROLOGY

# Propofol-induced loss of consciousness is associated with a decrease in thalamocortical connectivity in humans

Mahsa Malekmohammadi,[1] Collin M. Price,[1] Andrew E. Hudson,[2] Jasmine A.T. DiCesare[1] and Nader Pouratian[1]

Although the molecular effects of many anaesthetics have been well characterized, a network-level explanation for how these changes lead to loss of consciousness remains unclear. Studies using electroencephalography have characterized changes in neural oscillations in the cortex at specific frequency bands during propofol-induced anaesthesia and modelling work suggests these changes result from changes in thalamocortical functional connectivity. However, it is unclear if the neurophysiological changes seen at the cortex are due to enhanced or disrupted thalamocortical communication. Direct recordings from these sites during anaesthesia that could be used to confirm such models are rare. We recorded local field potentials from the ventral intermediate nucleus of the thalamus and electrocorticography signals from the ipsilateral sensorimotor cortex in 10 patients undergoing deep brain stimulation surgery. Signals were acquired during induction of propofol anaesthesia while subjects were resting. After confirming direct structural connectivity between the thalamus and the cortical recording site, we investigated propofol-associated changes in thalamic and cortical local power as well as thalamocortical functional connectivity, as measured with coherence, debiased weighted phase lag index, and phase amplitude coupling. Propofol anaesthesia resulted in local power increases at α frequencies (8–12 Hz) across both thalamic and cortical areas. At sensorimotor cortices, there was a broadband power increase (12–100 Hz), while the power of this same broad frequency band was suppressed within the thalamus. Despite the increase in local α power both within the thalamus and cortex, thalamocortical coherence and debiased weighted phase lag index in the α/low β frequencies (8–16 Hz, which was present in the awake state) significantly decreased with propofol administration ($P < 0.05$, two group test of coherence). Likewise, propofol administration resulted in decreased phase amplitude coupling between the phase of α/low β in the thalamus and the amplitude of broadband gamma (50–200 Hz) in the cortex ($P = 0.031$, Wilcoxon signed-rank test). We also report phase amplitude coupling between the phase of slow wave oscillations (0.1–1 Hz) and amplitude of broadband frequencies (8–200 Hz) within the cortex and across thalamocortical connections, during anaesthesia, both following a peak-max pattern. While confirming α-power increases with propofol administration both in thalamus and cortex, we observed decreased thalamocortical connectivity, contradicting models that suggest increasing cortical low frequency power is necessarily related to increased thalamocortical coherence but in support of the theory that propofol-induced loss of consciousness is associated with disrupted thalamocortical communication.

1 Department of Neurosurgery, University of California, Los Angeles, CA, USA
2 Department of Anaesthesiology, University of California, Los Angeles, CA, USA

Correspondence to: Mahsa Malekmohammadi, PhD
UCLA Neurosurgery, 300 Stein Plaza, Suite 464, Los Angeles, CA 90095, USA
E-mail: mmalekmohammadi@mednet.ucla.edu

Received September 25, 2018. Revised March 25, 2019. Accepted April 18, 2019. Advance Access publication June 24, 2019

**Keywords:** propofol; anaesthesia; thalamocortical; functional connectivity; electrophysiology

**Abbreviations:** DBS = deep brain stimulation; dWPLI = debiased weighted phase lag index; ECoG = electrocorticography; PAC = phase-amplitude coupling; SWO = slow wave oscillation; ViM = ventral intermediate

# Introduction

General anaesthesia is a transient state of unconsciousness that millions of individuals experience every year. While the action of anaesthetics at a molecular level has been well characterized, how this translates into the loss of consciousness is still incompletely understood (Lee and Mashour, 2018). This is particularly important in the clinical care of patients with neurological diseases as they can demonstrate differential patterns of responsiveness to anaesthetics. For example, patients with Parkinson disease demonstrate altered sensitivity to GABAergic anaesthetic agents such as propofol (Fábregas *et al.*, 2002; Xu *et al.*, 2015). On EEG, anaesthesia is generally marked by an increase in low frequency power ($<\sim$12 Hz) and a shift in the location of $\alpha$-oscillations from the occipital to the frontal cortex (Gugino *et al.*, 2001; Cimenser *et al.*, 2011; Purdon *et al.*, 2013; Ishizawa *et al.*, 2016; Guidera *et al.*, 2017). The appearance of this 'frontal $\alpha$' is a well-recognized and highly-studied phenomenon associated with anaesthetic-induced loss of consciousness, particularly with the intravenous anaesthetic propofol (Feshchenko *et al.*, 2004). The neurophysiological underpinnings of propofol-related changes in consciousness and the associated increase in cortical $\alpha$-power remain unclear, particularly as it relates to thalamocortical circuitry. Our goal is to use a unique opportunity to record invasively from the thalamocortical system in humans to determine whether behavioural and cortical neurophysiological changes seen with propofol administration are due to enhanced or diminished thalamocortical functional coupling. Unravelling the circuitry of anaesthesia-related loss of consciousness may impart important insights into our understanding of disorders of consciousness, for example, as posited by the meso-circuit model (Schiff, 2010).

A growing body of literature suggests that general anaesthesia is marked by a significant disruption of brain interregional communication (Hudetz, 2006; Lee *et al.*, 2009; Brown *et al.*, 2011; Schrouff *et al.*, 2011; Lewis *et al.*, 2012; Mashour and Alkire, 2013; Sarasso *et al.*, 2014). Some studies posit a central role of the thalamus in maintaining consciousness through communication with the cerebral cortex, suggesting anaesthesia targets the thalamocortical system (White and Alkire, 2003; Llinás and Ribary, 2006; Boveroux *et al.*, 2010; Liu *et al.*, 2013). Others suggest that anaesthesia mainly alters cortico-cortical communication (Velly *et al.*, 2007; Lee *et al.*, 2009; Schrouff *et al.*, 2011; Boly *et al.*, 2012), with changes in the thalamus simply reflecting decreased input from these cortical regions (Mashour and Alkire, 2013). In contrast to the theory of anaesthetic-related interruption of interregional coupling, a modelling study suggests that frontal $\alpha$ emerges from increased reciprocal coupling in the $\alpha$-band between thalamus and cortex as a result of the GABA-A potentiation elicited by propofol (Ching *et al.*, 2010). Mirroring the debate over whether unconsciousness is driven by changes in the cortex or thalamus, there is uncertainty as to whether the increase in the cortical $\alpha$-power is cortical (Velly *et al.*, 2007; Ching *et al.*, 2010; Vijayan *et al.*, 2013) or thalamic (Guidera *et al.*, 2017; Soplata *et al.*, 2017).

To assess anaesthetic-induced changes in cross-regional functional relationships, studies often use measures of coherence describing the correlation between the activity of these regions across various frequencies based on amplitude and phase (Fries, 2005). During anaesthesia, thalamocortical coherence has been reported to decrease in the β-band in humans (Swann *et al.*, 2016) and cortico-cortical networks (Malekmohammadi *et al.*, 2018*a*). However, recent invasive thalamocortical recordings in animals show different findings, indicating an increase in the thalamocortical coherence in the $\alpha$ and $\delta$ range in rats (Flores *et al.*, 2017). Part of the inconsistency may be related to the fact that the recording site in the thalamus largely varies across studies; anatomical parcellation of the thalamus and functional imaging studies suggest anaesthesia has varying effects on different thalamic nuclei (Liu *et al.*, 2013). Changes in thalamocortical coupling with anaesthesia, therefore, remain incompletely understood and characterized.

Recently, EEG studies of anaesthesia have also begun to describe the presence of cortical phase-amplitude coupling (PAC), in which the amplitude of a higher frequency band is constrained by the phase of another (Canolty and Knight, 2010). PAC is increasingly recognized as an important phenomenon as part of the normal and pathological neurophysiological function (Canolty and Knight, 2010; van der Meij *et al.*, 2012; de Hemptinne *et al.*, 2015; Malekmohammadi *et al.*, 2018*b*). As subjects transitioned to and from a state of propofol-induced unconsciousness, the amplitude of the cortical $\alpha/\beta$ activity was highest at the troughs of slow wave oscillations (SWO; with frequencies $< 1$ Hz), whereas during deep sedation with higher levels of propofol, the trend was reversed; that is, $\alpha/\beta$ amplitude was greatest during the peaks of low-frequency oscillations (Purdon *et al.*, 2013). Moreover, the transitionary 'trough-max' PAC signature was confined to the frontal cortex, while the steady state 'peak-max' PAC was observed throughout frontal, temporal and postcentral cortex (Mukamel *et al.*, 2014). Interestingly, human subjects with positive response to the isolated forearm test (IFT, a volitional response to a verbal command under propofol general anaesthesia), either show

no low frequency PAC or 'trough-max' PAC, but not the 'peak-max' PAC at the time of IFT, despite exhibiting the signature frontal cortical $\alpha$, indicating that classical EEG markers might not fully project the depth of anaesthesia (Gaskell *et al.*, 2017). Previously, we have reported, using invasive human recordings, of the presence of thalamocortical PAC, in which thalamic oscillations drive the amplitude of higher frequency cortical oscillations (Malekmohammadi *et al.*, 2015). Accordingly, recent modelling suggests that anaesthetic-induced changes in the thalamus may be responsible for these observed PAC patterns (Soplata *et al.*, 2017). However, these theories have not been formally tested with direct recordings in human brains from cortical and thalamic areas.

Despite extensive efforts and the advances described above, a coherent theory of anaesthetic-induced unconsciousness remains elusive, likely due in part to the contradictory findings in the field stemming from disparities in the method and location of recordings. Moreover, there are only a few studies that use direct human recordings to test the many theories and models put forward (such as cortico-centric or thalamic-centric theories). In this study, we provide a framework for studying anaesthetic-induced changes in the human thalamocortical system using a well-defined thalamocortical network with known structural connectivity. Specifically, we use invasive intracranial recordings to study the electrophysiology of the ventral-intermediate (ViM) nucleus of the thalamus and the sensory-motor cortex during anaesthesia.

After establishing structural connectivity between ViM and sensorimotor cortical areas using magnetic resonance diffusion tractography, we examine propofol-induced changes in local thalamic and cortical power as well as thalamocortical functional connectivity to assess the role of the thalamus in regulating cortical neurophysiological phenomena. Functional connectivity is evaluated using multiple measures of neurophysiological coupling including coherence and PAC as well as causality measures [debiased weighted phase lag index (dWPLI) and multivariate granger causality]. Together, these studies confirm (i) causal thalamocortical functional connectivity (in which the thalamic $\alpha$-band drives cortical oscillations) in the awake state; and (ii) propofol-induced loss of consciousness and changes in cortical physiology are related to loss rather than enhancement of thalamocortical functional connectivity.

# Materials and methods

## Patients and surgical procedure

Ten subjects with essential tremor undergoing bilateral ($n = 4$) or unilateral ($n = 6$) deep brain stimulation (DBS) lead implantation in the ViM nucleus of the thalamus, provided written informed consent according to the Declaration of Helsinki to participate in this study (Table 1). The study protocol was approved by the institutional review board of the University of California, Los Angeles. We recorded concurrent deep brain local field potentials (LFPs) from ViM thalamus and ipsilateral frontoparietal cortical electrocorticography (ECoG) (Fig. 1) during rest while subjects were undergoing awake DBS implantation and after intravenous administration of propofol.

All long-acting and short-acting medications were withdrawn at least 12 h prior to the surgery. Subjects underwent clinical pre- and postoperative imaging. Preoperative imaging included a $T_1$-weighted magnetization prepared rapid acquisition gradient echo (MPRAGE) image (slice thickness = 1 mm, 3 T, Siemens Skyra) and 64 direction diffusion tensor imaging (DTI) using single-shot spin echo echo-planar imaging (slice thickness = 3 mm, 3 T, Siemens Skyra). During the implantation procedure, a Leksell stereotactic head frame (Elekta Instruments) was applied to the skull and a full head CT scan was obtained using 1-mm slice thickness (Siemens Sensation 64). The DBS lead (Model 3387, 1.27 mm lead body diameter, contact length 1.5 mm, intercontact distance 1.5 mm, Medtronic, Inc) was targeted to the ViM, located 6 mm anterior to the posterior commissure, 11 mm lateral to the wall of the third ventricle, and at the anterior commissure-posterior commissure line. Intraoperative awake macro-stimulation testing was performed to confirm the clinically optimal final position of the DBS leads. Before implantation of the DBS leads, an eight-contact ECoG strip (platinum-iridium 4-mm contacts with 1-cm spacing; AdTech Medical) was temporarily introduced subdurally through the frontal burr hole placed for DBS lead implantation (left side for the unilateral left DBS cases and right side for unilateral right and bilateral DBS cases). The burr hole was always located within 1 cm (anterior or posterior) to the coronal structure. Given the length of the ECoG strip and the estimated location of the central sulcus (3–5 cm posterior to the coronal structure), the ECoG strip was guaranteed to span the sensory-motor area of the cortex. Location of DBS electrodes was confirmed using a single-view lateral fluoroscopy image captured after implantation of the DBS lead(s) as well as postoperative high resolution CT. The ECoG strip was removed after conducting the experiments and prior to final anchoring of the DBS leads.

## Experimental protocol

LFPs were recorded with the lead in final implant position in all subjects using the lead's four-ring electrode contacts (contacts 0, 1, 2 and 3, ventral to dorsal). Signal acquisition was carried out using BCI2000 v3 connected to an amplifier (g.Tec, g.USBamp 2.0) with a sampling rate of 2400 Hz and online 0.1–1000 Hz bandpass filtering. Ground and reference contacts were connected to the scalp. Bipolar re-referencing was used for further signal analysis.

We began recordings with patients resting awake with eyes open for 1 min, after which propofol was administered according to the attending anaesthesiologist's clinical judgement. Recordings continued and patients were assessed verbally at least every 15–30 s after propofol administration to ensure and determine the timing of loss of responsiveness. We used the modified observer's assessment of alertness/sedation scale (MOAA/S) to evaluate the subject's level of alertness. Each patient included in the study reached a score of 0/1, representing a state of no response or response only to a noxious stimulus, respectively, after which recordings continued for 1 min without further stimulation. Recordings continued for an

**Table 1 Cohort demographics and relevant clinical information**

| Subject code | Gender | Age | Weight, kg | Recording hemisphere | Hand dominance | Propofol bolus, mg | Propofol infusion rate, μg/kg/min | DBS contacts used for initial clinical programming Positive contact, negative contact, voltage (V)/pulse-width (μs)/stimulation frequency (Hz) |
|---|---|---|---|---|---|---|---|---|
| S1 | M | 76 | 96.2 | Right | Right | 60 | 70 | C+, 10–, 1.5/60/185 |
| S2 | F | 63 | 66.5 | Right | Right | 50 | 75 | C+, 10–, 0.7/60/180 |
| S3 | M | 79 | 110.4 | Right | Right | 0 | 100 | C+, 11–, 2.0/60/185 |
| S4 | M | 76 | 81 | Right | Right | 0 | 150 | C+, 9–, 1.0/60/185 |
| S5 | F | 67 | 95.8 | Left | Right | 50 | 200 | C+, 0–, 2.5/60/185 |
| S6 | M | 60 | 102.5 | Left | Right | 70 | 60 | C+, 2–, 1.5/60/185 |
| S7 | F | 67 | 99 | Left | Right | 25 | 75 | C+, 2–, 2.0/60/185 |
| S8 | F | 66 | 85.2 | Left | Right | 100 | 150 | C+, 1–, 2.0/60/185 |
| S9 | F | 75 | 54.4 | Right | Right | 30 | 80 | NA |
| S10 | F | 64 | 61.4 | Right | Left | 50 | 100 | C+, 9–, 1.2/60/185 |

NA = not available.

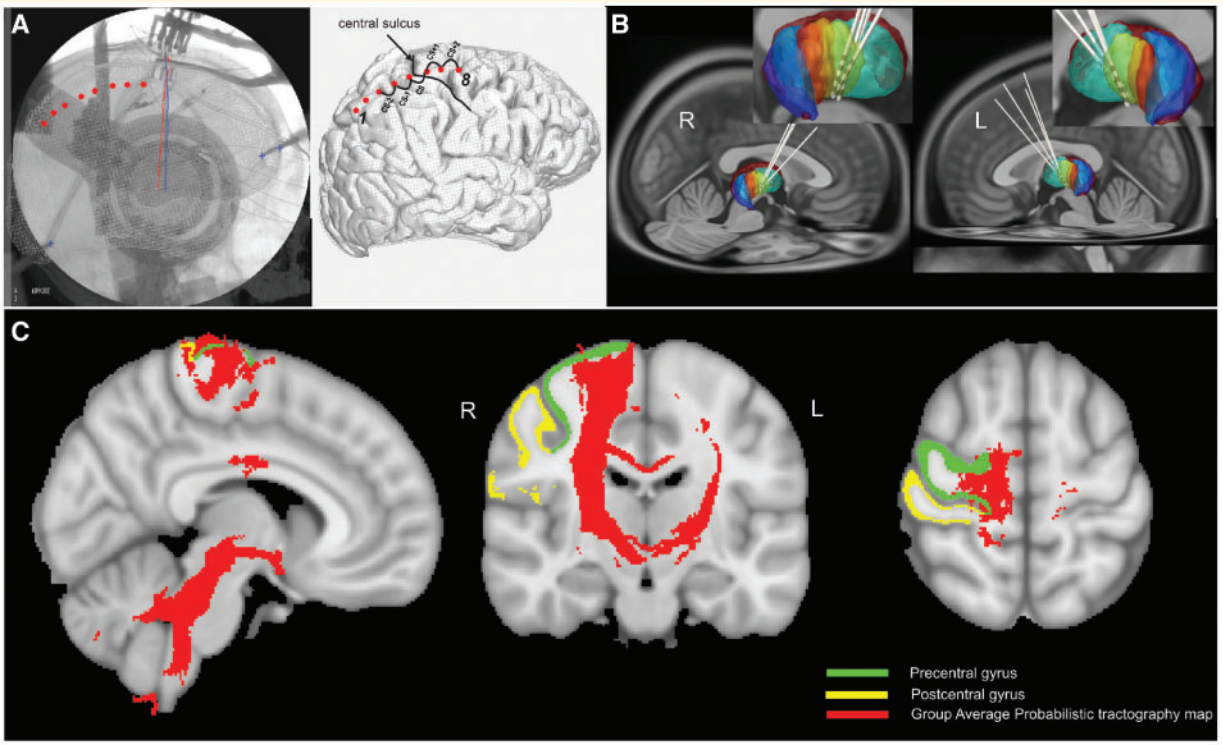


**Figure 1 Thalamic and cortical recording sites and interregional structural connectivity.** (**A**) The ECoG strip is localized over the cortical surface and contacts are marked for one subject. To represent relative location, each contact is named according to its position relative to CS, where CS – 1 and CS – 2 are electrode pairs 1 and 2 cm behind the CS pair, respectively, and CS + 1 and CS + 2 represent electrode pairs 1 and 2 cm anterior to the CS pair, respectively. (**B**) Leads used for DBS are reconstructed using the pre- and postoperative imaging and aggregated across the cohort ($n$ = 8, imaging not available for two subjects). Images are normalized to the standard brain and Oxford thalamic connectivity atlas is overlaid on the group image. This atlas divides the thalamus into seven functional zones based on the structural connectivity with colours coded as: dark blue: occipital cortex, light blue: post parietal cortex, cyan: prefrontal cortex, yellow: premotor cortex, orange: primary motor cortex, red: sensory cortex, dark red: temporal cortex. (**C**) Whole brain probabilistic tractography seeded from the most ventral contacts of the DBS lead, indicating preferential structural connectivity to the precentral gyrus and minimal connectivity to the postcentral gyrus. L = left; R = right.

average of 5 min after the start of propofol administration. Due to variations in propofol dosing, cardiac output, and blood volume across subjects, we expected substantial differences in circulation time and anaesthetic induction across subjects. Therefore, we focused our analyses on pre-bolus and post-induction steady state signals, using the last

minute of recording as the time period when subjects were maximally anaesthetized and no longer verbally responsive (hereafter referred to as 'anaesthesia period' or 'Anes'), and contrasted this with the pre-anaesthesia (pre-Anes) stage.

## Imaging data analysis

### Localization of ECoG strip and DBS electrodes

Anatomical localization of ECoG strip was carried out using a technique adopted from Randazzo *et al.* (2016) and described previously (Malekmohammadi *et al.*, 2018*a*). Briefly, pre- and postoperative CT scans co-registered to the preoperative high resolution structural MRI using normalized mutual information criteria, resliced in the Statistical Parameter Mapping (SPM) toolbox (SPM12), and visually inspected for accuracy. The cortical surface was reconstructed from the preoperative MPRAGE sequence MRI using Freesurfer. A 3D surface of the skull and stereotactic frame was rendered from the co-registered preoperative CT scan in the Osirix software. DBS electrodes were reconstructed from the co-registered postoperative CT scan and stereotactic frame landmarks were identified on the co-registered preoperative CT scan. The 2D fluoroscopic image and 3D skull surface were visually inspected and fused using a custom-made MATLAB graphical user interface and the camera toolbox. Reconstructed DBS leads and stereotactic frame landmarks were used to ensure maximal accuracy of 3D/2D fusion to the single-slice lateral fluoroscopy and localize the ECoG strip. After the localization concluded, the central sulcus (CS) was identified on the reconstructed cortical surface (Fig. 1A). The five overlying bipolar contacts were used for analysis across the cohort to cover pre and post-central gyri as well as parts of the frontal and parietal lobes. To represent relative location, each contact is named according to its position relative to central sulcus, where CS − 1 and CS − 2 are electrode pairs 1 and 2 cm behind the central sulcus pair, respectively, and CS + 1 and CS + 2 represent electrode pairs 1 and 2 cm anterior to the central sulcus pair, respectively (Fig. 1A). In two subjects with no postoperative CT scans, the central sulcus was identified using the median nerve somatosensory evoked potential reversal technique.

The DBS electrodes were localized using the Lead-DBS software (Horn and Kühn, 2015). Initially the postoperative CT scan was co-registered to the preoperative structural MRI using two-stage linear registration (rigid followed by affine) as implemented in advanced normalization tools (ANTs) (Avants *et al.*, 2008). Next, all images were normalized to the MNI standard stereotactic space (ICBM152 2009*b*, nonlinear asymmetric) using the SyN registration approach as implemented in ANTs (Avants *et al.*, 2008). Lead trajectories were pre-localized by Lead-DBS and manually adjusted to ensure optimal reconstruction in the standard space. Data from all patients were aggregated for visualization (Fig. 1A). Oxford thalamic connectivity atlas (Behrens *et al.*, 2003) was used to illustrate the relative position of the leads within the thalamus. Bipolar signals from contact pairs 0–1 were used for all of the analyses presented in this report.

### Probabilistic diffusion tractography

To delineate patterns of structural connectivity originating from the most ventral DBS bipolar contact (0–1), we carried out whole-brain probabilistic tractography (Behrens *et al.*, 2007). We used the postoperative CT scan (co-registered to the preoperative structural MRI) to define the seed mask. The centre point of the most ventral bipolar contact pairs (i.e. 0–1) was calculated based on the coordinates of the lowest tip of the electrode, and the angle between the electrode trajectory and sagittal and coronal planes and the lead geometry. The coordinates of the inter-contact distance were used as a centre point to create a 2-mm sphere seed mask. This seed mask was then co-registered to the preoperative diffusion space using linear transformations embedded in FLIRT (Jenkinson *et al.*, 2002) (mutual information as cost function, 6 degrees of freedom).

The DTI data were preprocessed by carrying out skull stripping and correction for eddy currents in the gradient coils and then a multi-fibre diffusion model was fitted to the data (BEDPOSTX) (Behrens *et al.*, 2007). Finally, we used this estimated diffusion model to perform probabilistic tractography between the seed mask and the rest of the brain (fsl PROBTRACKX2) using 5000 samples, a 0.2 curvature threshold, and loop-check termination. Resulting connectivity maps were then transferred to the preoperative structural space using transformation matrices generated before. For each patient, the map was divided by the overall number of streamlines and then binarized at 0.01 threshold value. For subjects with left DBS implantation, the binarized map was mirrored to the right hemisphere. All maps were then aggregated and averaged across subjects to create a shared connectivity map.

## Electrophysiological data analysis

### Data preprocessing

Signal analysis was carried out using custom made scripts in MATLAB (Version 8.6, The Mathworks Inc., Natick, MA) and Fieldtrip toolbox (Oostenveld *et al.*, 2010). Data were converted to bipolar montage and standardized using Z-transformation (to account for variable signal amplitude across cortical and subcortical signals and across the cohort) (AuYong *et al.*, 2018; Malekmohammadi *et al.*, 2018*c*) and parsed into pre-anaesthetic and anaesthetic epochs excluding all the segments containing electrical or unwanted movement artefact (Tsiokos *et al.*, 2017). Removed segments primarily featured power spectra with abnormally high values, excessive harmonics and time series with high rates of voltage change. Data were bandpass filtered at 0.3–300 Hz using a two-way least-squares FIR filter (eegfilt.m; forward and backward to ensure no phase distortion). Line noise (60 Hz) and its harmonics (up to 300 Hz) were removed from the data using a bandstop filter with 2 Hz bandwidth and centred at the line noise frequency (and the following harmonics) as implemented in the fieldtrip toolbox.

### Power spectral density

Power spectral density (PSD) for pre-anaesthetic and anaesthetic conditions was calculated using the Thomson's multitaper method in 1-s consecutive time windows with no overlap for frequencies of 0.3 to 300 Hz with ± 2 Hz frequency bandwidth (T = 1 s, W = 2, and K = 2TW − 1 = 3 tapers) (Bokil *et al.*, 2010). Group average PSDs for both conditions were then calculated at each contact pair.

## Magnitude squared coherence and phase connectivity

We used magnitude squared coherence to explore cortical-subcortical synchrony. The magnitude squared coherence was calculated between ipsilateral ViM and cortical signals using Thomson's multitaper method with similar parameters as the PSD analysis. To confirm that coherence results do not represent spurious volume conduction, we used a measure of phase connectivity shown to be unaffected by the effects of a common source. After measuring power spectra, we calculated cross-spectral density for each thalamocortical signal pair, using similar time and frequency resolution as spectral and coherence analysis. The dWPLI was then calculated for all of the frequencies of interest (0.3–300 Hz) (Vinck *et al.*, 2011). The dWPLI measures the non-equiprobability of phase leads and lags between the two signals and has been shown to be insensitive to the effects of volume conduction from independent sources or active reference (Vinck *et al.*, 2011).

### Phase amplitude coupling

PAC was estimated using Tort's method of modulation index (MI) (Tort *et al.*, 2010; Malekmohammadi *et al.*, 2015). Parameters selected for PAC analysis were chosen based on recommendations from a previous critical analyses of PAC methodology (Aru *et al.*, 2015). Briefly, signals were bandpass filtered using a two-way least squares FIR filtering (phase: 0.3–35 Hz, in 1-Hz steps and 2 Hz bandwidth; amplitude: 1–300 Hz in 2-Hz steps and double the phase-encoding frequency). Hilbert transform was then used to extract the instantaneous phase and amplitude of the two components, respectively. Phase values were then binned (18 bins, 20° width) and the mean amplitude distribution was calculated relative to the phase bins to create a phase-amplitude histogram. Kullback-Leibler divergence was used to measure the deviation of this histogram from a uniform distribution and create MI values. In order to extract the preferred phase, for each frequency pair (phase and amplitude), the weights of the phase-amplitude histogram were used as amplitudes of a vector, while the centre phase of each bin constituted the phase of the vector.

To measure the tendency of the maximum 8–200 Hz amplitude to occur at the peaks of SWO phase, we calculated the $P_{max}I$ (Gaskell *et al.*, 2017). Briefly signals were bandpass filtered using similar filter as described above (phase: 0.3–1 Hz, amplitude: 8–200 Hz), instantaneous phase and amplitude and phase-amplitude histogram were calculated. A peak-max coupling tends to have the maximum amplitude when the SWO phase is ~0°; whereas the trough-max pattern shows maximum amplitude when the SWO phase is close to 180°. Therefore we calculated the $P_{max}I$ as the ratio of mean amplitude in bins 7–12, divided by the mean amplitude in bins 1–3 and 16–18. $P_{max}I > 1$ and $P_{max}I < 1$ indicates peak-max and trough-max coupling, respectively.

### Multivariate Granger causality

We used frequency domain Granger causal inference to explore directional functional connectivity between thalamic and cortical signals as implemented in the multivariate Granger causality (MVGC) toolbox (Barnett and Seth, 2014). Granger causality is based on the predictability and precedence, assuming that cause precedes and helps predict the effect. We used signals from three nodes: ViM, and the contacts corresponding to 1 cm anterior and 1 cm posterior to central sulcus; we chose non-adjacent cortical signals to minimize the effect of shared signals on the multivariate model.

To optimize the selection of model order for the vector autoregressive (VAR) model, we first downsampled the preprocessed data to 300 Hz. To meet the stationarity condition of data we divided our signals into 1-s windows with 50% overlap. Then, the Bayesian information criterion (BIC) was used to estimate model order. A VAR model was constructed using the selected model order (=25) using Levinson, Wiggins and Robinson (LWR) algorithm (Morf *et al.*, 1978), and the auto-covariance sequence was calculated from the VAR parameters. Finally, pairwise conditional Granger causality in the frequency domain was calculated from the auto-covariance sequence (Barnett and Seth, 2014). The frequency resolution of the granger prediction is determined by the model order. Our selection of the model order was such to provide enough frequency resolution to capture at least one full cycle of $\alpha$ frequencies (~10 Hz). The same model order was used across the cohorts and conditions to avoid bias in statistical comparisons.

## Statistical analysis

Statistical analysis was carried out using MATLAB and SPSS statistical software (IBM Corp.). Statistically significant differences in spectral power/coherence between two conditions (pre-anaesthetic and anaesthetic) at each frequency was assessed using the two-group test of the spectrum/coherence (Bokil *et al.*, 2007), with a null hypothesis that both conditions have equal spectra/coherence. Our choice of the two-group test was based on the asymptotic probability distributions (Bokil *et al.*, 2007; Malekmohammadi *et al.*, 2018*a*) and Jackknife correction of the difference z-scores. This method is advantageous for its correction of bias inherent to the estimation process. As multitaper analysis uses an orthogonal family of tapers (i.e. Slepian sequences) over non-overlapping windows, the calculated tapered spectra/coherence can be reasonably assumed to be statistically independent. We derived the mean group spectra/coherence for both conditions along with the corresponding Z statistics and the 95% confidence intervals (CIs), based on the Jackknife estimation of variance (Bokil *et al.*, 2007). To correct for multiple comparisons, we note that differences in spectra/coherence due to chance are likely to be at discrete frequencies, while neurophysiological differences span contiguous frequency ranges. As spectral/coherence estimates at frequencies separated by less than the bandwidth of the multitaper method (4 Hz) are inherently correlated, we rejected the null hypothesis for all candidate frequencies constituting bands with width > 4 Hz (Goldfine *et al.*, 2011).

To assess the statistical significance of the PAC values, surrogate data analysis using a shuffling procedure was carried out. For each signal pair, we generated 1000 temporally shuffled versions of phase signals and calculated MI-values for each. The true MI-value was converted to a Z-score and the false discovery rate (FDR) procedure was used with $q = 0.05$ to adjust the corresponding *P*-values and correct for multiple comparisons (Benjamini *et al.*, 2001; Genovese *et al.*, 2002). Average PAC was calculated for distinct frequency band pairs and used for further statistical analyses across the population.

We used non-parametric permutation testing to explore the statistical difference of the dWPLI and frequency domain granger causality across the cohort between the two conditions. At each permutation ($n$ = 1000), a random subset of the pool was selected for which the labels of the conditions were swapped, creating a null distribution of the group difference. As the difference values at each frequency bin were bound between −1 and 1, we used Fisher Z-transform to construct an approximately normal distribution of the condition difference under the null hypothesis (Cohen, 2014). The significance of the condition difference was then assessed at $P = 0.05$ and corrected for multiple comparisons in a similar fashion to the spectral and coherence analyses.

## Data availability

All data included in this manuscript will be available upon reasonable request to the authors.

# Results

## Anatomical localization of DBS leads and structural connectivity to the precentral gyrus

First, we confirmed the anatomical location of the implanted DBS leads using the methods described above (Fig. 1B). This analysis confirmed desired placement of thalamic leads and cortical strips, with the thalamic atlas (Behrens *et al.*, 2003) overlying the most ventral contact pair indicating higher probability of connectivity to the precentral gyrus (Pouratian *et al.*, 2011; Tsolaki *et al.*, 2018). Probabilistic diffusion tractography further confirmed that fibres seeded from the most ventral contact pair on the DBS lead (i.e. contact 0–1) exhibit strong structural connectivity to the pre-central gyrus and brainstem/cerebellum (Fig. 1C). Exemplary raw signal traces from one sample subject (S4) is shown in Fig. 2A.

## Propofol differentially modulates local power in thalamic and cortical nodes

To characterize changes in local neuronal activity near each contact, we calculated changes in PSDs between pre-anaesthetic and anaesthetic conditions (Fig. 2B and C). After propofol administration, we observed a global increase in low frequency power (< 12 Hz) in the thalamus and at all cortical contact pairs. Above 12 Hz, power changes became discordant between thalamus and cortex. While thalamic power decreased during anaesthesia for all frequencies > 12 Hz, we observed an increase in power up to ~100 Hz in all cortical contacts except the most posterior one.

## Thalamocortical α and β functional connectivity is suppressed with propofol

We observed significant pre-anaesthesia coherence in the α/low-β band (9–19 Hz) between thalamus and sensorimotor cortical contacts (Fig. 3A). In addition, we found significant high-β coherence (23–31 Hz) between the thalamus and parietal/sensory contacts (Fig. 3A). No significant thalamocortical coherence was found for other frequencies (⩽300 Hz) (Supplementary Fig. 2).

Next, we assessed anaesthesia-induced changes in thalamocortical functional connectivity by looking at changes in coherence and dWPLI between ViM and each cortical contact pair. We observed significantly decreased coherence after anaesthesia induction in the α/low-β frequency band (10–17 Hz) at cortical contacts near the central sulcus. Of note, despite finding a decrease, we still observed significant residual coherence in this band at the pre-central gyrus and central sulcus (Fig. 3A). Likewise, the high-β coherence between ViM and posterior cortical contacts was suppressed with propofol (26–31 Hz; Fig. 3A). We also observed dWPLI changes at similar frequency bands, most notably with significant anaesthesia-induced decreases in α/low-β at contacts near the central sulcus, and high-β band decreases near sensory cortex (Fig. 3B).

Frequency domain multivariate causality analysis showed that α/low-β and high-β causality were significantly higher from ViM to sensorimotor cortices compared to the opposite direction (i.e. from sensorimotor cortex to the thalamus, Fig. 3B). The Granger causality analysis indicated that α/low-β and high-β band oscillations from the ViM were acting as a driver of information flow to cortical signals. The thalamocortical Granger causality is significantly smaller (in both directions) during the anaesthetic period compared to the pre-anaesthetic period.

Given that α coherence values (Fig. 3A) are comparable across the cortical sites (CS − 1 cm, CS and CS + 1 cm) while α dWPLI values are smaller at CS + 1 cm compared to CS and CS − 1 cm, we can argue that ViM − (CS + 1 cm) coherence could be due to volume conduction. The α coherence could be due to the presence of a common source of this signal to both ViM and (CS + 1 cm). Both CS and CS + 1 cm share a common contact on the motor cortex and our tractography analysis indicate dominant structural connectivity between the ViM and motor cortex, which then could act as the common source of α coherence in the premotor area.

To ensure that analyses of power and connectivity were not biased by the choice of windowing parameters, we tested the effect of window length on the power and coherence/PLI results using similar windowing parameters as reported by Flores and colleagues (2017) [T = 2 s with 1 s overlap and TW = 3 (W = 1.5 Hz) for five tapers] (Supplementary Fig. 1A) and others (Goldfine *et al.*, 2011; Guidera *et al.*, 2017) (T = 3 s with no overlap and half-bandwidth of (W = 1 Hz)/2 Hz spectral resolution, resulting in five tapers) (Supplementary Fig. 1B).

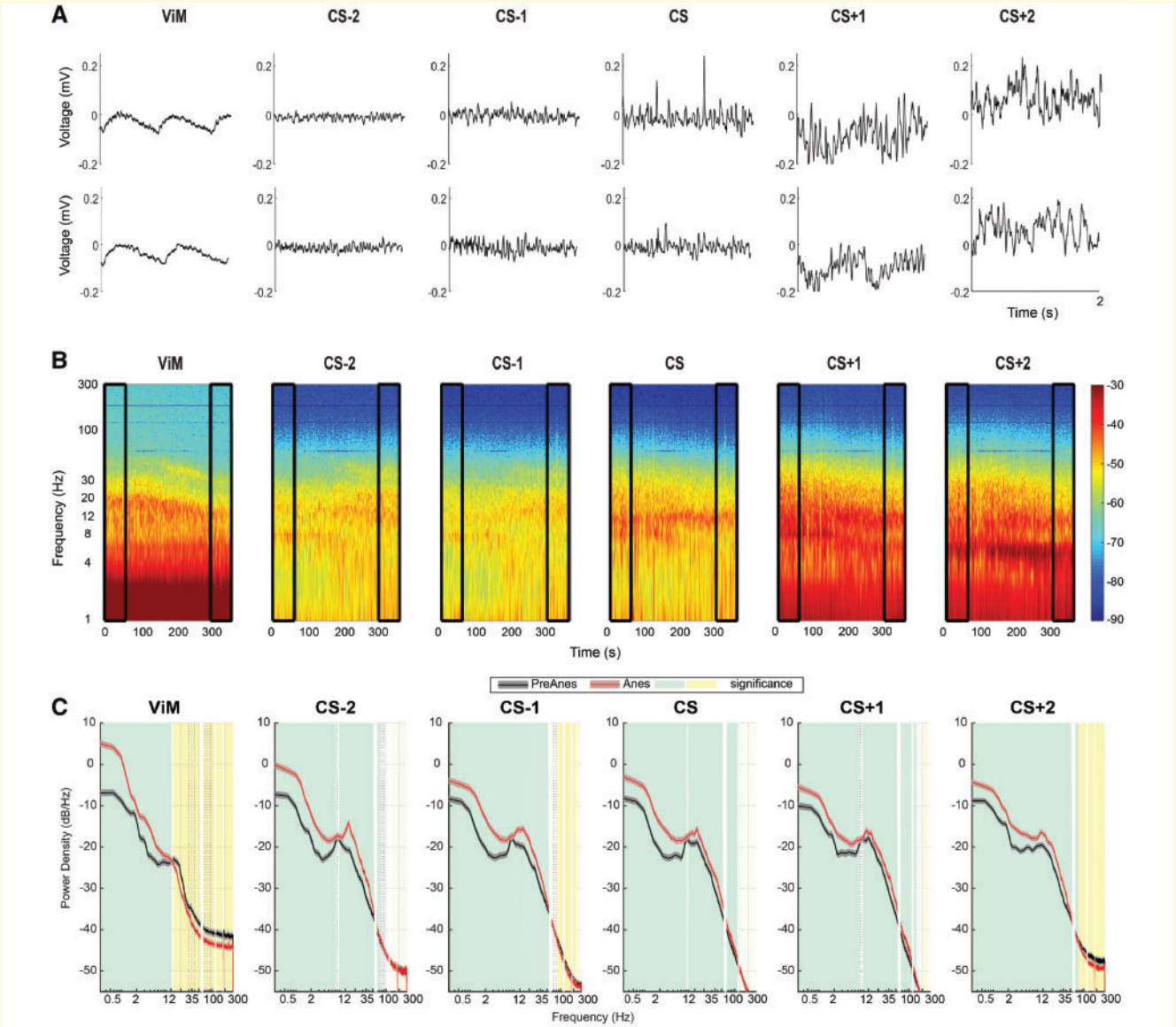


**Figure 2 Example of raw data traces and changes in local spectral power in the thalamus and cortical sites.** (**A**) Exemplary raw signal traces from one sample subject across all thalamic and cortical recording sites [*top* panel showing signals during pre-anaesthesia (PreAnes) wakefulness and *bottom* panel showing signals during the anaesthetized (Anes) state]. (**B**) Time frequency power spectral maps during the entire recording period for the same subject shown in **A**, indicating how power at different frequencies evolves during the transition from resting state wakefulness to the anaesthetized state. Black boxes on the *left*/*right* of each map show the time frame used for pre/post-anaesthesia analyses. (**C**) Six panels show power spectral densities (PSDs) for frequencies between 0.3 and 300 Hz for each location, averaged across all participants. The time axis is shown in a logarithmic scale to magnify changes in low frequencies. Same-colour shading around each PSD curve indicates 95% CI of the average. Green/yellow shadings indicate significantly increased/decreased power during anaesthesia ($P < 0.05$ and corrected for multiple comparisons).

## Propofol suppresses cortical α/low-β PAC while increasing slow wave oscillation PAC

We investigated how anaesthesia affected thalamocortical and cortico-cortical functional connectivity by calculating changes in PAC between all recording sites. The group average PAC for the cortical signal overlaying the central sulcus is demonstrated in Fig. 4A, revealing two significant patterns. First, across multiple regions, we observed a decrease in coupling during anaesthesia between the phase of the α/low-β band and the amplitude of broadband gamma (50–200 Hz). The most notable decreases in PAC were in

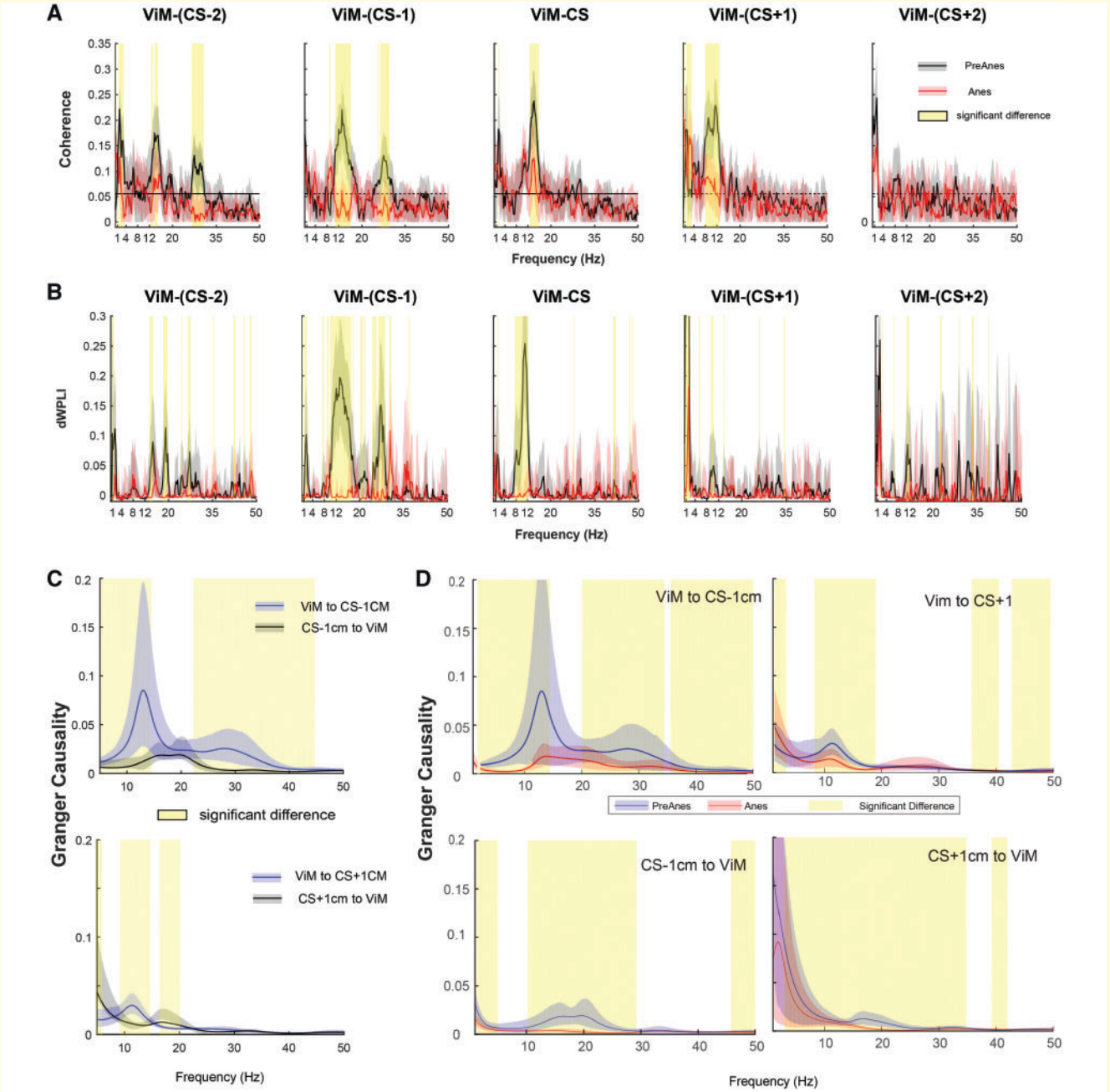


**Figure 3 Changes in thalamocortical coherence, phase-based connectivity and conditional multivariate Granger causality.** (**A**) The pairwise magnitude squared coherence between the ViM nucleus of the thalamus and each cortical contact spanning ± 2 cm around the central sulcus, for frequencies between 1 and 50 Hz. Same-colour shading around each coherence curve indicates 95% CI of the average. Yellow shading indicates significant ($P < 0.05$) suppression of coherence during anaesthesia period. (**B**) dWPLI for the same signal pairs and frequency range as illustrated in **A**. Same-colour shading around each dWPLI curve indicates 95% CI of the average. Yellow shading indicates significant ($P < 0.05$) suppression of dWPLI during the anaesthesia period. (**C**) Pair-wise conditional multivariate Granger causality (MVGC) between ViM and post-central (*top*) and precentral (*bottom*) cortical signals. Same-colour shading around each curve indicates 95% CI of the average. Yellow shading indicates significant ($P < 0.05$) difference between thalamocortical and cortico-thalamic flow, corrected for multiple comparisons. (**D**) Comparison of MVGC during wakefulness and anaesthetized state, indicating suppression of causal signal flow between the thalamus and cortical areas during anaesthesia. Yellow shading indicates significant ($P < 0.05$) difference corrected for multiple comparisons.

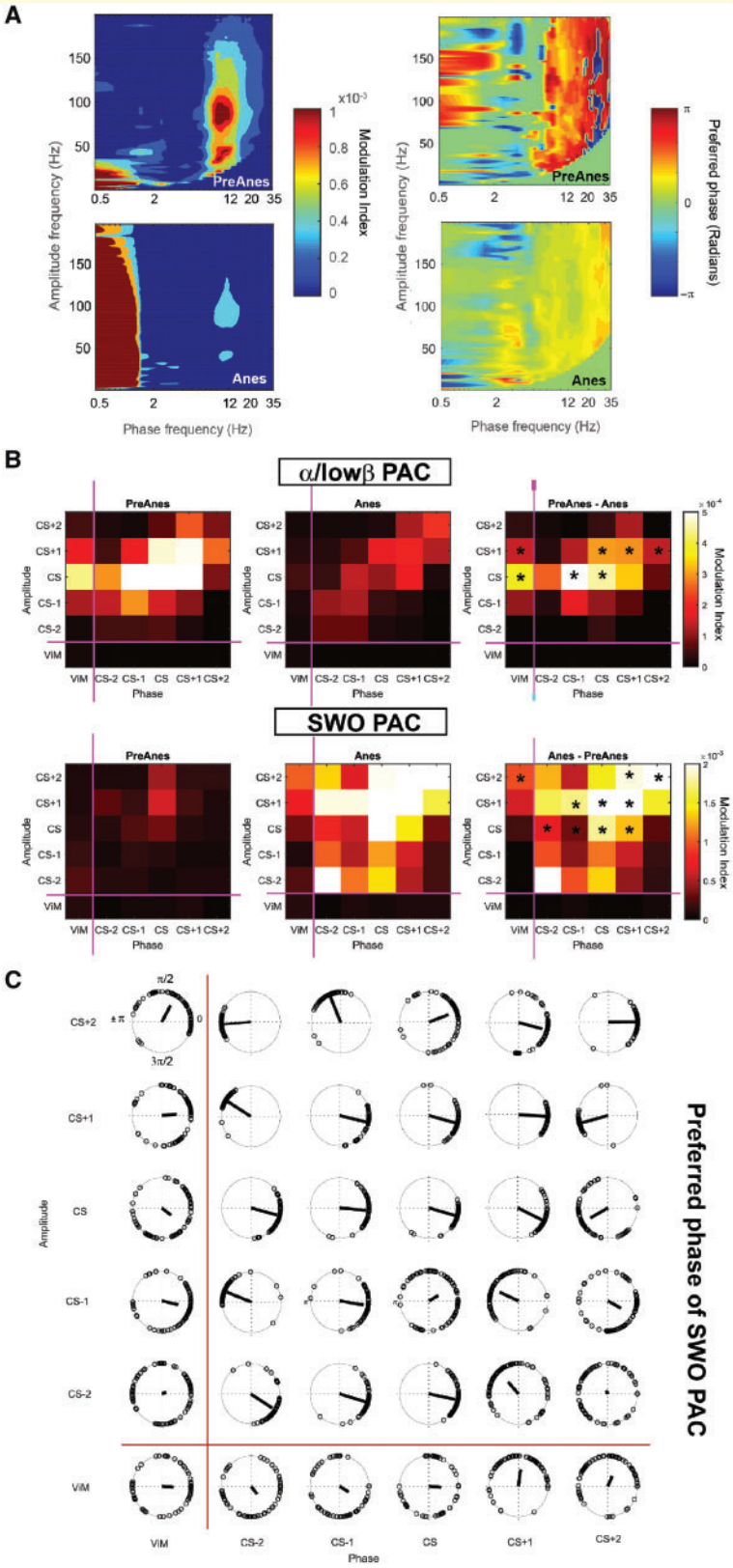


**Figure 4 Changes in thalamocortical local and cross-site phase amplitude coupling (PAC).** (**A**) Group average PAC heat map for the cortical signal overlaying the precentral gyrus during baseline (*top*) and after induction of anaesthesia (*bottom*). (**B**) Grids illustrate group average PAC between $\alpha$/low $\beta$-phase and $\gamma$-amplitude (*top row*) and PAC between SWO phase and amplitude of for frequencies between 8–200 Hz (*bottom row*). Grids are calculated for baseline (PreAnes) and during anaesthesia (Anes) conditions and the difference between the two conditions are shown in the grid on the *right*. Changes in average PAC values are compared and significant difference is illustrated by an asterisk ($P < 0.05$). (**C**) The group average circular distribution of the preferred phase for the SWO coupling across amplitude frequencies during the anaesthetic (Anes) period, indicating a preferred phase centred on zero (corresponding to a peak-max pattern). PreAnes = pre-anaesthetic.

the phase of ViM modulating the amplitude of cortex, and in the phase of central sulcus/precentral gyrus modulating the amplitude of other cortical contacts (Fig. 4B, top). To quantify these PAC differences, we binned frequencies into $\alpha$ and high-β/low-gamma bands. Figure 4B illustrates localization of significant decreases in this PAC pattern.

Second, we observed an increase in coupling after anaesthesia induction, between the phase of SWO (0.3–1 Hz) and frequencies across a broad band from 8–200 Hz. This pattern was observed predominantly in the cortex as an increase in caudal-to-rostral coupling, with the phase of posterior contacts modulating the amplitude of anterior contacts (Fig. 4B). The anaesthesia-induced increase in SWO-broadband PAC was also observed between the phase of ViM and the amplitude of frontal cortical contacts. To quantify this PAC difference, we binned frequencies into SWO and broadband bands. Figure 4B illustrates localization of significant increases in this PAC pattern.

The group average preferred phase PAC for the cortical signal overlaying the central sulcus is shown in Fig. 4A, indicating that the preferred coupling phase was close to zero radians for SWO coupling during anaesthesia. This preferred phase was consistent across the broad range of amplitude frequencies (8–200 Hz) as indicated in Fig. 4C, which shows the circular distribution of the preferred phase for the SWO coupling across amplitude frequencies during the anaesthetic period.

The $P_{max}I$-values were on average $> 1$ for ViM-frontal cortical SWO-broadband couplings (1.16, range: 0.91–1.91, $P = 0.02$, Wilcoxon signed-rank test) indicating the presence of 'peak-max' pattern such that the amplitude of broadband oscillations was maximal at the zero phase of SWO. For corticocortical coupling, $P_{max}I$ averaged across the subjects was on average 1.05 (range: 0.91–1.21), given that we have considered a grid of corticocortical PAC (Fig. 4B), further breakdown of the $P_{max}I$ values based on the contacts indicated that coupling of phase component from posterior contacts (sensory cortex) to the amplitude of anterior contacts (motor areas) was significantly $> 1$ (1.11, range: 0.91–1.22, $P < 0.05$, Wilcoxon signed-rank), indicating a similar 'peak-max' pattern.

# Discussion

Confirming prior studies, we observed an anaesthesia-induced increase in low frequency ($< 12$ Hz) power at all thalamic and cortical recording sites, a common finding in both cortex (Velly *et al.*, 2007; Breshears *et al.*, 2010; Cimenser *et al.*, 2011; Mhuircheartaigh *et al.*, 2013; Purdon *et al.*, 2013; Mukamel *et al.*, 2014; Swann *et al.*, 2016; Ishizawa *et al.*, 2016; Guidera *et al.*, 2017) and thalamus (Velly *et al.*, 2007; Verdonck *et al.*, 2014; Swann *et al.*, 2016; Flores *et al.*, 2017; Guidera *et al.*, 2017). While the increase in the cortical $\alpha$-activity may in part be related to eye closure, which is associated with widespread cortical power increases in the $\alpha$-band and low frequencies (Geller *et al.*, 2014), this is a potential confound of all studies of the effects of anaesthesia. We also found a decrease in high frequency power ($> 12$ Hz) in the thalamus, which has been observed during anaesthesia using invasive recordings in both animals (Zhang *et al.*, 2014; Reed and Plourde, 2015; Plourde *et al.*, 2016) and humans (Velly *et al.*, 2007; Verdonck *et al.*, 2014; Swann *et al.*, 2016). These findings together have been purported to represent an overall decrease in neuronal activity in these regions (Swann *et al.*, 2016). A decrease in thalamic $\gamma$-power, in particular, is consistent with previous findings showing decreased blood oxygen level-dependent (BOLD) signal in the thalamus, measured by functional MRI (Boveroux *et al.*, 2010; Liu *et al.*, 2013; Mhuircheartaigh *et al.*, 2013), considering the BOLD signal has been found to be congruent with high frequency power (Lachaux *et al.*, 2007; Ojemann *et al.*, 2013). While these observations confirm prior work as well as the validity of the current recordings, concomitant changes in thalamocortical functional coupling provided the greatest novel insights.

The current analyses provide direct evidence that propofol-induced loss of consciousness and changes in cortical physiology are related to loss rather than potentiation of thalamocortical functional connectivity, as measured with coherence and cross-site PAC. The observed decrease in thalamocortical $\alpha$-coherence is contrary to modelling work (Ching *et al.*, 2010; Vijayan *et al.*, 2013) and invasive recordings in rats (Flores *et al.*, 2017; Guidera *et al.*, 2017) reporting increased $\alpha$-coherence. Although one could argue that changes in $\alpha$-power in each region could affect coherence, the observed changes in dWPLI at the same frequency imply that the coherence changes are due to changes in the phase relationship. The observed decrease in $\alpha$-coherence is also interesting in light of the decrease in $\alpha$/lowβ PAC. This PAC pattern was strong in the pre-anaesthesia state between the thalamus and central sulcus/pre-central gyrus as well as between central sulcus and other regions of cortex (Fig. 4B). In nearly every region pair where this pattern existed, it was completely abolished with propofol. The decreased thalamocortical $\alpha$-coherence during anaesthesia suggests thalamus may be the source of this potentially crucial PAC pattern. Therefore, cortical $\alpha$ phase-encoded PAC (rather than $\alpha$-power) may be an important biomarker of thalamocortical connectivity and arousal.

One explanation for the discrepancies in findings of thalamocortical connectivity with propofol administration may lie in differences in recording sites. While some studies examining the effect of anaesthesia on the thalamus have treated the entire region as one unit (Velly *et al.*, 2007; Swann *et al.*, 2016), others have recognized the important differences in connectivity and function of thalamic nuclei (Llinás and Ribary, 2006; Liu *et al.*, 2013; Mashour and Alkire, 2013; Baker *et al.*, 2014). An important distinction has been made between the non-specific nuclei of the intralaminar thalamus, responsible for the integration of cortical information, and the specific nuclei in other regions of the thalamus, responsible for the transmission of the motor and

sensory signals (Jones, 2001; Llinás and Ribary, 2006; Theyel *et al.*, 2010; Mashour and Alkire, 2013). Investigators using the BOLD signal in humans (Liu *et al.*, 2013) and invasive recordings in rats (Baker *et al.*, 2014) have reported that changes in the non-specific nuclei with anaesthesia precede changes in the specific nuclei and are better correlated with measures of loss-of-consciousness. Here we report decreased $\alpha$-coherence between cortex and one of the specific nuclei (ViM), while studies showing increased $\alpha$-coherence have been measured from central thalamus (Flores *et al.*, 2017; Guidera *et al.*, 2017).

While $\alpha$-coherence was decreased between structurally connected regions of thalamus and cortex (as demonstrated by magnetic resonance tractography), we observed other patterns of coherence changes that may be related to differential patterns of structural connectivity. Specifically, β-band coherence was seen only between the thalamus and sensory cortex during the pre-anaesthesia state and was completely abolished with anaesthesia. Notably, we saw no β-coherence between motor cortex and thalamus, in contrast to a previous study using invasive recordings in similar patients (Swann *et al.*, 2016). Based on our lead localization and tractography analyses, the thalamic recording sites have less dominant structural connectivity to sensory cortex. Thus, the coherence between these regions represents functional connectivity that may be mediated by one of two alternate structural pathways: (i) corticocortical connections between motor and sensory cortex; or (ii) intrathalamic connections between ViM and sensory-projecting thalamic nuclei. While motor and sensory cortex are reciprocally connected, we argue that intrathalamic connectivity is more likely. First, Granger causality analysis revealed that the high β-coherence represented ViM driving the flow of information in cortical signals. In addition, we would expect a cortically-mediated connection (from thalamus to motor cortex to sensory cortex) to result in some β-band coherence at baseline between thalamus and motor cortex. The fact that we observed no such coherence argues for an intrathalamic structural pathway facilitating functional connectivity between ViM and sensory cortex. Interestingly, Guidera *et al.* (2017) observed a similar decrease in β-band coherence that coincided with loss of movement in anaesthetized rats; however, their recordings were between prefrontal cortex and central thalamus.

The difference in the degree to which propofol modulated $\alpha$-coherence (significantly reduced but still preserved) in the motor thalamocortical circuit in contrast to the complete loss of β-coherence in the sensory circuit is also noteworthy. This is consistent with recent resting state functional MRI work in monkeys, which showed functional connectivity became proportionally constrained to structural connectivity maps with increasing levels of anaesthesia (Barttfeld *et al.*, 2015; Uhrig *et al.*, 2018). In other words, anaesthesia may have a stronger effect on functional connectivity between regions that lack structural connectivity.

We also observed an anaesthesia-induced increase in coupling between the phase of SWO and the amplitude of $\alpha$ across the cortex following a peak-max pattern similar to the previous studies (Purdon *et al.*, 2013; Mukamel *et al.*, 2014; Gaskell *et al.*, 2017; Soplata *et al.*, 2017). However, in addition to what prior EEG work suggests, we found coupling between the phase of SWO and the amplitude of a broad range of frequencies from 8 to 200 Hz, rather than just the $\alpha$-band, which may have been due to the sensitivity to higher frequencies enabled by ECoG recordings compared to EEG. More interestingly for the first time, we observed this increased PAC between thalamus and cortex, similarly with a peak-max pattern, supporting the modelling studies suggesting a thalamic origin for the SWO phase (Soplata *et al.*, 2017).

Our novel finding of increased SWO-broadband PAC in the thalamocortical system during anaesthesia is particularly interesting considering the work of Lewis *et al.* (2012). Using ECoG and single-electrode data from three patients with epilepsy, they found a robust marker of anaesthesia characterized by periods of neuronal firing increase and suppression coupled to the peaks/troughs of the SWO phase, respectively. They also demonstrated that the SWO phase of different cortical regions became less synchronized with increasing distance between them (Lewis *et al.*, 2012). Our finding of increased coupling of broadband activity to SWO phase may represent these periods of on/off neuronal spiking, which they reported, in a patient population with completely different pathology. In addition, this spatial and temporal fragmentation may also explain why some studies, including the present one, have found increased $\gamma$-power over the cortex (Baker *et al.*, 2014; Malekmohammadi *et al.*, 2018*a*), while others have found a decrease (Breshears *et al.*, 2010; Verdonck *et al.*, 2014; Zhang *et al.*, 2014; Pal *et al.*, 2015; Reed and Plourde, 2015; Plourde *et al.*, 2016); depending on the recording location and temporal resolution, the spatially disparate and time-varied increases in power may be lost. The spatial segregation of propofol effects on cortical activity are highlighted in Fig. 2 in which differential patterns of changes in high frequency activity are noted across cortical sites, with more pronounced decreases in the most anterior recording areas (corresponding to the motor and premotor areas).

Importantly, the differential pattern of propofol-related changes in functional connectivity across thalamocortical recording sites highlights the importance of simultaneously assessing structural and functional connectivity and carefully considering different patterns of spectrally-specific functional changes that may be observed across distinct regions of cortex and thalamus.

## Limitations

Limitations in invasive human neurophysiological studies necessarily arise from clinical considerations. As with nearly all invasive neurophysiological studies in humans,

our data were restricted to patients with significant neuropathology. Our thalamic recordings, by ethical necessity, originate from a region implicated in the disease process of our patients. Therefore, it is unknown whether reported changes in signal dynamics are merely related to the motor system or whether these changes would generalize to other thalamocortical circuitry as a generalizable phenomenon of maintenance/loss of consciousness.

In addition, in patients with movement disorders, one can reasonably expect some alterations in the normal activity of the motor cortex. Indeed, previous work has identified increases in cortical $\alpha/\beta$ power in patients with essential tremor (Crowell *et al.*, 2012; Rowland *et al.*, 2015). Despite the underlying neurological disease, our results largely corroborate and expand upon previous findings in animals or patients without movement disorders. Likewise, the method of anaesthesia administration and monitoring in this study was based on the clinical judgement of the anaesthesiologist. While these settings preclude detailed investigations of dose-dependent effects or the transitional anaesthetized state, we attempted to mitigate these shortcomings by examining the steady states prior to and after induction of anaesthesia. Ultimately, studies can and should be conducted to better understand how these various measures of local and network activity relate to both the depth of anaesthesia as well as the evolution of changes in consciousness with anaesthetic administration. Essentially, within-subject dose-response studies should and need to be conducted. Likewise, a comparison of anaesthesia induction to anaesthesia recovery, as has been carried out recently (Breshears *et al.*, 2010; Hwang *et al.*, 2012; Flores *et al.*, 2017) should be pursued. In addition, due to clinical timing and recording constraints, we were limited to 1-min artefact-free data during pre- and post-anaesthesia periods and as such, all the segments included in the final analyses were 60 s long. While a longer segment of data is preferable while examining sub-Hz frequency activity, our results highlight that changes in spectral power and functional connectivity (PAC) in low frequencies are consistent during the 1 min post-anaesthesia recordings and with that previously reported in the literature. Fortunately, the current work provides and characterizes a human model for acquiring data and testing hypotheses in human subjects that can be used for future studies.

# Funding

This work was supported by the National Institutes of Biomedical Imaging and Bioengineering [K23EB014326], National Institutes of Neurological Disorders and Stroke [R01NS097782], philanthropic support from Casa Colina Centers for Rehabilitation. M.M. was supported by postdoctoral fellowship from American Parkinson disease association (APDA, NY, USA) and A.H. was supported by National Institutes of General Medical Sciences (K08GM121961).

# Competing interests

The authors report no competing interests.

# Supplementary material

Supplementary material is available at *Brain* online.

# References

Aru JJ, Aru JJ, Priesemann V, Wibral M, Lana L, Pipa G, et al. Untangling cross-frequency coupling in neuroscience. Curr Opin Neurobiol 2015; 31: 51–61.

AuYong N, Malekmohammadi M, Ricks-Oddie J, Pouratian N. Movement-modulation of local power and phase amplitude coupling in bilateral globus pallidus interna in Parkinson disease. Front Hum Neurosci 2018; 12: 270.

Avants BB, Epstein CL, Grossman M, Gee JC. Symmetric diffeomorphic image registration with cross-correlation: evaluating automated labeling of elderly and neurodegenerative brain. Med Image Anal 2008; 12: 26–41.

Baker R, Gent TC, Yang Q, Parker S, Vyssotski AL, Wisden W, et al. Altered activity in the central medial thalamus precedes changes in the neocortex during transitions into both sleep and propofol anesthesia. J Neurosci 2014; 34: 13326–35.

Barnett L, Seth AK. The MVGC multivariate Granger causality toolbox: a new approach to Granger-causal inference. J Neurosci Methods 2014; 223: 50–68.

Barttfeld P, Uhrig L, Sitt JD, Sigman M, Jarraya B, Dehaene S. Signature of consciousness in the dynamics of resting-state brain activity. Proc Natl Acad Sci USA 2015; 112: 887–92.

Behrens TEJ, Berg HJ, Jbabdi S, Rushworth MFS, Woolrich MW. Probabilistic diffusion tractography with multiple fibre orientations: what can we gain? Neuroimage 2007; 34: 144–55.

Behrens TEJ, Johansen-Berg H, Woolrich MW, Smith SM, Wheeler-Kingshott CAM, Boulby PA, et al. Non-invasive mapping of connections between human thalamus and cortex using diffusion imaging. Nat Neurosci 2003; 6: 750–7.

Benjamini Y, Drai D, Elmer G, Kafkafi N, Golani I. Controlling the false discovery rate in behavior genetics research. Behav Brain Res 2001; 125: 279–84.

Bokil H, Andrews P, Kulkarni JE, Mehta S, Mitra PP. Chronux: a platform for analyzing neural signals. J Neurosci Methods 2010; 192: 146–51.

Bokil H, Purpura K, Schoffelen JM, Thomson D, Mitra P. Comparing spectra and coherences for groups of unequal size. J Neurosci Methods 2007; 159: 337–45.

Boly M, Moran R, Murphy M, Boveroux P, Bruno MA, Noirhomme Q, et al. Connectivity changes underlying spectral EEG changes during propofol-induced loss of consciousness. J Neurosci 2012; 32: 7082–90.

Boveroux P, Vanhaudenhuyse A, Bruno M-A, Noirhomme Q, Lauwick S, Luxen A, et al. Breakdown of within- and between-network resting state functional magnetic resonance imaging connectivity during propofol-induced loss of consciousness. Anesthesiology 2010; 113: 1038–53.

Breshears JD, Roland JL, Sharma M, Gaona CM, Freudenburg ZV, Tempelhoff R, et al. Stable and dynamic cortical electrophysiology

of induction and emergence with propofol anesthesia. Proc Natl Acad Sci USA 2010; 107: 21170–5.
Brown EN, Purdon PL, Van Dort CJ. General anesthesia and altered states of arousal: a systems neuroscience analysis. Annu Rev Neurosci 2011; 34: 601–28.
Canolty RT, Knight RT. The functional role of cross-frequency coupling. Trends Cogn Sci 2010; 14: 506–15.
Ching SN, Cimenser A, Purdon PL, Brown EN, Kopell NJ. Thalamocortical model for a propofol-induced alpha-rhythm associated with loss of consciousness. Proc Natl Acad Sci USA 2010; 107: 22665–70.
Cimenser A, Purdon PL, Pierce ET, Walsh JL, Salazar-Gomez AF, Harrell PG, et al. Tracking brain states under general anesthesia by using global coherence analysis. Proc Natl Acad Sci USA 2011; 108: 8832–7.
Cohen XM. Analyzing neural time series data. Cambridge, MA: MIT Press; 2014.
Crowell AL, Ryapolova-Webb ES, Ostrem JL, Galifianakis NB, Shimamoto S, Lim DA, et al. Oscillations in sensorimotor cortex in movement disorders: an electrocorticography study. Brain 2012; 135: 615–30.
de Hemptinne C, Swann NC, Ostrem JL, Ryapolova-Webb ES, San Luciano M, Galifianakis NB, et al. Therapeutic deep brain stimulation reduces cortical phase-amplitude coupling in Parkinson's disease. Nat Neurosci 2015; 18: 779–86.
Fábregas N, Rapado J, Gambús PL, Valero R, Carrero E, Salvador L, et al. Modeling of the sedative and airway obstruction effects of propofol in patients with Parkinson disease undergoing stereotactic surgery. Anesthesiology 2002; 97: 1378–86.
Feshchenko VA, Veselis RA, Reinsel RA. Propofol-induced alpha rhythm. Neuropsychobiology 2004; 50: 257–66.
Flores FJ, Hartnack KE, Fath AB, Kim S-E, Wilson MA, Brown EN, et al. Thalamocortical synchronization during induction and emergence from propofol-induced unconsciousness. Proc Natl Acad Sci 2017; 114: 6660–8.
Fries P. A mechanism for cognitive dynamics: neuronal communication through neuronal coherence. Trends Cogn Sci 2005; 9: 474–80.
Gaskell AL, Hight DF, Winders J, Tran G, Defresne A, Bonhomme V, et al. Frontal alpha-delta EEG does not preclude volitional response during anaesthesia: prospective cohort study of the isolated forearm technique. Br J Anaesth 2017; 126: 371–2.
Geller AS, Burke JF, Sperling MR, Sharan AD, Litt B, Baltuch GH, et al. Eye closure causes widespread low-frequency power increase and focal gamma attenuation in the human electrocorticogram. Clin Neurophysiol 2014; 125: 1764–73.
Genovese CR, Lazar NA, Nichols T. Thresholding of statistical maps in functional neuroimaging using the false discovery rate. Neuroimage 2002; 15: 870–8.
Goldfine AM, Victor JD, Conte MM, Bardin JC, Schiff ND. Determination of awareness in patients with severe brain injury using EEG power spectral analysis [Internet]. 2011. Available from: https://pdfs.semanticscholar.org/0d6f/02a798c45392739394c34010def746b29f24.pdf (10 August 2017, date last accessed).
Gugino LD, Chabot RJ, Prichep LS, John ER, Formanek V, Aglio LS. Quantitative EEG changes associated with loss and return of consciousness in healthy adult volunteers anaesthetized with propofol or sevoflurane. Br J Anaesth 2001; 87: 421–8.
Guidera JA, Taylor NE, Lee JT, Vlasov KY, Pei J, Stephen EP, et al. Sevoflurane induces coherent slow-delta oscillations in rats. Front Neural Circuits 2017; 11.
Horn A, Kühn AA. Lead-DBS: a toolbox for deep brain stimulation electrode localizations and visualizations. Neuroimage 2015; 107: 127–35.
Hudetz AG. Suppressing consciousness: mechanisms of general anesthesia. Semin Anesth Perioper Med Pain 2006; 25: 196–204.
Hwang E, Kim S, Han K, Choi JH, Ward LM. Characterization of phase transition in the thalamocortical system during anesthesia-induced loss of consciousness. PLoS One 2012; 7: e50580.
Ishizawa Y, Ahmed OJ, Patel SR, Gale JT, Sierra-Mercado D, Brown EN, et al. Dynamics of propofol-induced loss of consciousness across primate neocortex. J Neurosci 2016; 36: 7718–26.
Jenkinson M, Bannister P, Brady M, Smith S. Improved optimization for the robust and accurate linear registration and motion correction of brain images. Neuroimage 2002; 17: 825–41.
Jones EG. The thalamic matrix and thalamocortical synchrony. Trends Neurosci 2001; 24: 595–601.
Lachaux JP, Fonlupt P, Kahane P, Minotti L, Hoffmann D, Bertrand O, et al. Relationship between task-related gamma oscillations and BOLD signal: new insights from combined fMRI and intracranial EEG. Hum Brain Mapp 2007; 28: 1368–75.
Lee U, Kim S, Noh GJ, Choi BM, Hwang E, Mashour GA. The directionality and functional organization of frontoparietal connectivity during consciousness and anesthesia in humans. Conscious Cogn 2009; 18: 1069–78.
Lee U, Mashour GA. Role of network science in the study of anesthetic state transitions. Anesthesiology 2018; 129: 1029–44.
Lewis LD, Weiner VS, Mukamel EA, Donoghue JA, Eskandar EN, Madsen JR, et al. Rapid fragmentation of neuronal networks at the onset of propofol-induced unconsciousness. Proc Natl Acad Sci USA 2012; 109: E3377–86.
Liu X, Lauer KK, Ward BD, Li SJ, Hudetz AG. Differential effects of deep sedation with propofol on the specific and nonspecific thalamocortical systems: a functional magnetic resonance imaging study. Anesthesiology 2013; 118: 59–69.
Llinás R, Ribary U. Consciousness and the Brain. Ann N Y Acad Sci 2006; 929: 166–75.
Malekmohammadi M, AuYong N, Price CM, Tsolaki E, Hudson AE, Pouratian N. Propofol-induced changes in α-β sensorimotor cortical connectivity. Anesthesiology 2018a; 128: 305–16.
Malekmohammadi M, AuYong N, Ricks-Oddie J, Bordelon Y, Pouratian N. Pallidal deep brain stimulation modulates excessive cortical high β phase amplitude coupling in Parkinson disease. Brain Stimul 2018b; 11: 607–17.
Malekmohammadi M, Elias WJJ, Pouratian N. Human thalamus regulates cortical activity via spatially specific and structurally constrained phase-amplitude coupling. Cereb Cortex 2015; 25: 1618–28.
Malekmohammadi M, Shahriari Y, AuYong N, O'Keeffe A, Bordelon Y, Hu X, et al. Pallidal stimulation in Parkinson disease differentially modulates local and network $\beta$ activity. J Neural Eng 2018c; 15: 056016.
Mashour GA, Alkire MT. Consciousness, anesthesia, and the thalamocortical system. Anesthesiology 2013; 118: 13–5.
Mhuircheartaigh RN, Warnaby C, Rogers R, Jbabdi S, Tracey I. Slow-wave activity saturation and thalamocortical isolation during propofol anesthesia in humans. Sci Transl Med 2013; 5: 208ra148.
Morf M, Vieira A, L. Lee D, Kailath T. Recursive multichannel maximum entropy spectral estimation. IEEE Trans Geosci Electron 1978; 16: 85–94.
Mukamel EA, Pirondini E, Babadi B, Wong KFK, Pierce ET, Harrell PG, et al. A transition in brain state during propofol-induced unconsciousness. J Neurosci 2014; 34: 839–45.
Ojemann G, Ojemann J, Ramsey NF. Relation between functional magnetic resonance imaging (fMRI) and single neuron, local field potential (LFP) and electrocorticography (ECoG) activity in human cortex. Front Hum Neurosci 2013; 7: 34.
Oostenveld R, Fries P, Maris E, Schoffelen J-M, Oostenveld R, Fries P, et al. FieldTrip: Open source software for advanced analysis of MEG, EEG, and invasive electrophysiological data, fieldtrip: open source software for advanced analysis of MEG, EEG, and invasive electrophysiological data. Comput Intell Neurosci Comput Intell Neurosci 2011; 2011: e156869.

Pal D, Hambrecht-Wiedbusch VS, Silverstein BH, Mashour GA. Electroencephalographic coherence and cortical acetylcholine during ketamine-induced unconsciousness. Br J Anaesth 2015; 114: 979–89.

Plourde G, Reed SJ, Chapman CA. Attenuation of high-frequency (50–200 Hz) thalamocortical electroencephalographic rhythms by isoflurane in rats is more pronounced for the thalamus than for the cortex. Anesth Analg 2016; 122: 1818–25.

Pouratian N, Zheng Z, Bari AA, Behnke E, Elias WJ, DeSalles AAF. Multi-institutional evaluation of deep brain stimulation targeting using probabilistic connectivity-based thalamic segmentation. J Neurosurg 2011; 115: 995–1004.

Purdon PL, Pierce ET, Mukamel EA, Prerau MJ, Walsh JL, Wong KF, et al. Electroencephalogram signatures of loss and recovery of consciousness from propofol. Proc Natl Acad Sci USA 2013; 110: E1142–51.

Randazzo MJ, Kondylis ED, Alhourani A, Wozny TA, Lipski WJ, Crammond DJ, et al. Three-dimensional localization of cortical electrodes in deep brain stimulation surgery from intraoperative fluoroscopy. Neuroimage 2016; 125: 515–21.

Reed SJ, Plourde G. Attenuation of high-frequency (50–200 Hz) thalamocortical EEG rhythms by propofol in rats is more pronounced for the thalamus than for the cortex. PLoS One 2015; 10: e0123287.

Rowland NC, De Hemptinne C, Swann NC, Qasim S, Miocinovic S, Ostrem JL, et al. Task-related activity in sensorimotor cortex in Parkinson's disease and essential tremor: changes in beta and gamma bands. Front Hum Neurosci 2015; 9: 512.

Sarasso S, Rosanova M, Casali AG, Casarotto S, Fecchio M, Boly M, et al. Quantifying cortical EEG responses to TMS in (un)consciousness. Clin EEG Neurosci 2014; 45: 40–9.

Schiff ND. Recovery of consciousness after brain injury: a mesocircuit hypothesis. Trends Neurosci 2010; 33: 1–9.

Schrouff J, Perlbarg V, Boly M, Marrelec G, Boveroux P, Vanhaudenhuyse A, et al. Brain functional integration decreases during propofol-induced loss of consciousness. Neuroimage 2011; 57: 198–205.

Soplata AE, McCarthy MM, Sherfey J, Lee S, Purdon PL, Brown EN, et al. Thalamocortical control of propofol phase-amplitude coupling. PLoS Comput Biol 2017; 13: e1005879.

Swann NC, de Hemptinne C, Maher RB, Stapleton CA, Meng L, Gelb AW, et al. Motor system interactions in the beta band decrease during loss of consciousness. J Cogn Neurosci 2016; 28: 84–95.

Theyel BB, Lee CC, Sherman SM. Specific and nonspecific thalamocortical connectivity in the auditory and somatosensory thalamocortical slices. Neuroreport 2010; 21: 861–4.

Tort ABL, Komorowski R, Eichenbaum H, Kopell N. Measuring phase-amplitude coupling between neuronal oscillations of different frequencies. J Neurophysiol 2010; 104: 1195–210.

Tsiokos C, Malekmohammadi M, AuYong N, Pouratian N. Pallidal low β-low $\gamma$ phase-amplitude coupling inversely correlates with Parkinson disease symptoms. Clin Neurophysiol 2017; 128: 2165–78.

Tsolaki E, Downes A, Speier W, Elias WJ, Pouratian N. The potential value of probabilistic tractography-based for MR-guided focused ultrasound thalamotomy for essential tremor. NeuroImage Clin 2018; 17: 1019–27.

Uhrig L, Sitt JD, Jacob A, Tasserie J, Barttfeld P, Dupont M, et al. Resting-state dynamics as a cortical signature of anesthesia in monkeys. Anesthesiology 2018; 129: 942–58.

van der Meij R, Kahana M, Maris E. Phase-amplitude coupling in human electrocorticography is spatially distributed and phase diverse. J Neurosci 2012; 32: 111–23.

Velly LJ, Rey MF, Bruder NJ, Gouvitsos FA, Witjas T, Regis JM, et al. Differential dynamic of action on cortical and subcortical structures of anesthetic agents during induction of anesthesia. Anesthesiology 2007; 107: 202–12.

Verdonck O, Reed SJ, Hall J, Gotman J, Plourde G. The sensory thalamus and cerebral motor cortex are affected concurrently during induction of anesthesia with propofol: a case series with intracranial electroencephalogram recordings. Can J Anesth 2014; 61: 254–62.

Vijayan S, Ching S, Purdon PL, Brown EN, Kopell NJ. Thalamocortical mechanisms for the anteriorization of alpha rhythms during propofol-induced unconsciousness. J Neurosci 2013; 33: 11070–5.

Vinck M, Oostenveld R, van Wingerden M, Battaglia F, Pennartz CM. An improved index of phase-synchronization for electrophysiological data in the presence of volume-conduction, noise and sample-size bias. Neuroimage 2011; 55: 1548–65.

White NS, Alkire MT. Impaired thalamocortical connectivity in humans during general-anesthetic-induced unconsciousness. Neuroimage 2003; 19: 402–11.

Xu X, Yu X, Wu X, Hu X, Chen J, Li J, et al. Propofol requirement for induction of unconsciousness is reduced in patients with Parkinson's disease: a case control study. Biomed Res Int 2015; 2015: 953729.

Zhang Y, Li Z, Dong H, Yu T. Effects of general anesthesia with propofol on thalamocortical sensory processing in rats. J Pharmacol Sci 2014; 126: 370–81.